Journal of Structural Dynamics

Squeal occurrence classification using a harmonic balance vector signal model

Etienne Balmes [*1,2], Guillaume Martin[†2], Guilherme Malacrida Alves[2,1], and Guillaume Vermot des Roches[‡2]

[1] *ENSAM, CNRS, CNAM, PIMM, 151 Boulevard de l'hopital, Paris, France*
[2] *SDTools, 44 Rue Vergniaud, Paris, France*

Abstract

Brake squeal is an instability that generates self-excited limit cycles which vary with time and operating conditions in real experiments. To analyze test results, it is proposed to use a Harmonic Balance Vector (HBV) signal model. It combines Harmonic Balance Method and analytic signal methodologies. From the Harmonic Balance Method, one uses the space-time decomposition where spatial distribution of each harmonic is described by a complex vector and frequency is common to all sensors. From analytic signal, one keeps the assumption that quantities are slowly varying in time. Synchronous demodulation and principal coordinate definitions are combined in a multistep algorithm that provides an HBV estimation.

On an industrial brake test matrix, HBV estimation is shown to be robustly applicable. The HBV signal being slowly varying, time sub-sampling reduces the volume of test data by two orders of magnitude. Limit cycle frequency, amplitude and shapes can thus be added to the parallel coordinates that associate to each time sample the operating parameters: pressure, velocity, temperature, torque, disk position, disk/bracket distance, ... This opens a path to a range of analyzes otherwise difficult to perform. Classification of squeal occurrences is first discussed showing pressure and amplitude dependence. The effect of amplitude on both frequency and shape is next demonstrated. The entry and exit of instability when parameters change are then analyzed by proposing a transient root locus built from test. Thus squeal test results are related to the classical complex eigenvalue analysis. Intermittent growth/decay events are shown to be correlated with wheel position. Furthermore, distance measurements indicate that disk shape variations of a few microns play a clear parametric role. Parametric testing and clustering are then used to map the instability region and its edges. Pressure is shown to have an effect dominating other variations. Prospective uses of these results to combine test results and finite element models are discussed last.

Keywords: Analytic signal; Harmonic Balance; time varying non-linear system; squeal classification; brake

Received on January 23, 2025, Accepted on March 26, 2025, Published on March 31, 2025

1 Introduction

Brake squeal is a friction induced instability by mode coupling [1], that leads to high amplitude limit cycles. The phenomenon has been extensively studied, experimentally, see references [2, 3] among many, and numerically from minimal models [4] to industrial models [5]. Due to the phenomenon complexity, a characterization rationale has yet to be defined.

[*] etienne.balmes@ensam.eu
[†] martin@sdtools.com
[‡] vermot@sdtools.com

Extraction of squeal features for variable operating conditions, which will be described by *parameters* here, is a clear need illustrated in [6]. Feature extraction for creep groan phenomenon classification has also been performed in [7]. Features classically include frequencies of limit cycles, both acoustic and vibration amplitudes. Shape will also be included here as it allows fine distinctions of occurrences and is useful to perform numerical correlation. Properly selecting parameters and features is necessary for efficient datalakes feeding for further design studies.

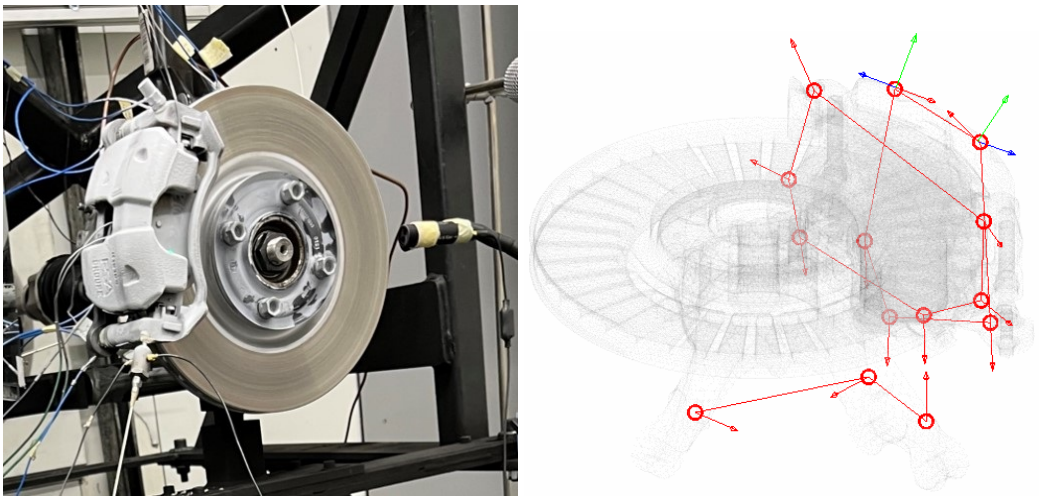

Fig. 1: Left: measurement setup. Right: accelerometer positionning on the brake.

Figure 1 illustrates the industrial brake configuration considered here and the sensor configuration that is used to define squeal shape vectors. More details about the setup and the experiments will be given in section 3, but at this point one only notes that a non production pad design was chosen for its clear propensity to squeal.

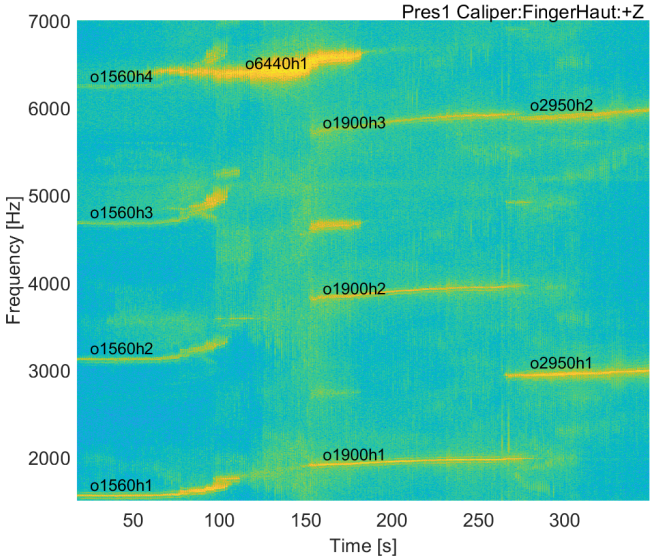

Fig. 2: Acceleration spectrogram during an increasing pressure, constant velocity, experiment

Figure 2 illustrates a pressure sensitivity characterization experiment, where pressure is ramped manually in the range $P = [1.5 - 9]$ bar while velocity is kept constant (drag mode). The system changes slowly as piston pressure is increased. The spectrogram clearly illustrates a first limit cycle near 1560 Hz and 4 harmonics shown using labels (for instance o1560h3 refers to the third harmonic of squeal occurrence whose fundamental frequency is close to 1560Hz). Between 60 and 120s, harmonic 4 interacts with harmonic 1 of another limit cycle near 6440 Hz. Another transition then occurs, ... Non-linear vibration studies typically focus on those transitions, and more details would be expected. But the present work focuses on providing a signal model suitable for automated classification of squeal experiments, so the purpose of the figure is only to illustrate requirements which are listed below.

- **Propose a signal model representing the main squeal features**. Squeal induces limit cycles, thus the response is close to being periodic and dominated by harmonics (that will be described by a Harmonic Balance Vector HBV detailed later), but other broadband noise exists due to passage of asperities below the pad, as will be illustrated in section 3.3. It is thus desirable to be able to separate both signal types in raw measurements.
- **Track the squeal limit cycle changes**. The frequency of the limit cycles is not known and evolves over time faster than possible tracking using standard short time Fourier transform methods. It must thus be reliably estimated with times scales that will be discussed in section 2.1. Squeal is not permanent so that tracking must account for the fact that other excitation sources may dominate the response at certain times.
- **Reduce data while preserving main vibration features**. Keeping all channels of raw time data generates too much data (10 GB for the 20 minutes discussed in section 3.1) and makes classification difficult. Obtaining slowly varying features (limit cycle frequency, amplitude, and shape) sampled at the rate of parameter changes is thus fundamental.
- **Make the link between limit cycle changes and operational parameters**. Parameters known to have a major influence are pressure, temperature, wheel angle [8] and velocity, wear [9, 10], loaded pad settling position which is influenced by the braking history, ... But, as discussed in section 2.1, those parameters vary slowly enough to consider a frequency separation with the limit cycle.
- **Relate test and FEM results**. Experimental and numerical brake squeal state-of-the-art methods do not rely on the same analyzes. Experimental results focus on non-linear high amplitude limit cycle measurements whereas numerical methods focus on unstable complex modes valid for low amplitude vibrations where the model is linearized around a static state (even with FEM model reduction, transient simulation methods so far remain too costly to be used in design). Despite the discrepancy, knowing the associated underlying shapes is useful for remediation work based on an understanding of how components deform. However, since squeal occurs at relatively high frequencies, analysis purely based on sensors is difficult and combining test and FEM may be useful for understanding as discussed in section 3.5.

The harmonic balance method [11, 12, 13, 14, 15] is a classical strategy to search periodic solutions of non-linear systems. HBM is based on a space/time discretization of responses as a series of complex spatial vectors and integer harmonics of a base frequency. HBM is typically considered as a numeric tool allowing the transformation of non-linear differential problems into algebraic systems of equation, whose solution is a state vector combining amplitudes of all kept harmonics. Frequency is either a driving parameter for forced responses or an additional state in the case of self excited vibrations such as squeal [13]. Here, the state vector will be called Harmonic Balance Vector (HBV) and will be used to analyze experiments.

Experimentally, harmonics are often analyzed using discrete Fourier transforms with very well known trade-off between buffer length and frequency resolution, or wavelets that require fine-tuning. To go beyond these limitations, analytic signals [16], assume a complex q_a signal of the form

$$q_a(t) = q_1(t)e^{i\varphi(t)} = q_1(t)e^{i\int_t \omega(t)dt} \tag{1}$$

where the real part of the signal is the measured signal $q(t)$, the imaginary part is the Hilbert transform of $q(t)$, $q_1(t)$ is the real amplitude and $\varphi(t)$ the phase which can be interpreted as the integral of a variable frequency $\omega(t)$. Demodulation strategies considered in many real time applications [17, 18, 19, 20, 21] have shown their practical robustness and will be adapted here. Spectrum reassignment techniques [22, 23] are another class of methods dealing with discrete Fourier limitations and might be considered.

The claim of section 2 is that it is relevant to combine HBM and analytic signal ideas, and consider the HBV as a signal model to analyze experiments. While clearly inspired by developments of analytic signal methods [16, 24], the HBV naming insist on specific signal features. The instantaneous frequency is common to all sensors. The response associated to a single frequency is a complex vector, it should thus occur within a rank 2 manifold/subspace corresponding to the real and imaginary parts of HBM solutions. If the system varies slowly, the instantaneous frequency and shape also vary slowly, so that timescale separation can help proper estimation. Section 2 discusses the combination of classical methodologies chosen to estimate a signal verifying these properties.

As a support of the claim that these considerations are useful, section 3 analyzes results of a squeal test campaign on the industrial brake shown in Figure 1. Section 3.2 first discusses squeal parameters and features. Needs associated with their estimation in realistic configurations are then addressed. Finally, their use for occurrence classification using frequency amplitude and possibly shape clustering is detailed. Section 3.3 then seeks to a draw a parallel between numerical parametric studies of complex modes, called root locus in control theory, and values

to be extracted from experiments. To allow refined characterization of the instability area and its edges, section 3.4 proposes to use parametric testing by varying pressure, which is the parameter with first order influence. Section 3.5 finally discusses how the proposed results can be used in conjunction with finite element simulations.

2 HBV signal description

2.1 Definition and outline of estimation strategy

In the present case of a brake squeal limit cycle, and more generally for the periodic forced response of a non-linear system, one expects that over a short enough time, the system can be considered invariant and harmonic balance may allow a correct estimation of solutions. The Harmonic Balance state Vector (HBV), that will be used for signal estimation, combines the response at model DOF or measured sensors $\{q_h\}$ (where the vector nature is show by the $\{\ \}$ notation and h is the integer harmonic index) and the instantaneous frequency ω common to all spatial components and harmonics. A key assumption is that these parameters vary slowly in time, leading to the signal model

$$\{q_{HBV}(\omega(t_{slow}), q_h(t_{slow}))\} = \sum_{h\in\mathcal{H}} Re\left(\{q_h(t_{slow})\}\, e^{ih\varphi(t)}\right) = \sum_{h\in\mathcal{H}} Re\left(\{q_h(t_{slow})\}\, e^{ih\int_0^t \omega(t_{slow})dt}\right) \tag{2}$$

where the rapidly varying instantaneous phase is the time integral of the slowly varying instantaneous frequency $\varphi(t) = \int_0^t \omega(t_{slow})dt$.

The ability to distinguish slow and fast time scales depends on a frequency separation illustrated in Figure 3. The limit cycle around 3 kHz defines the fast timescale. Slower variations are a drive shaft torsion mode around 30 Hz (in one of the test bench used), the wheel spin typically below 1 Hz for the speeds of interest, the steps associated with pressure ramps, and the gradual increase of temperature. The frequency separation, by two orders of magnitude here, is a property that seems essential for the successful estimation of an HBV signal. Geometric changes that will be illustrated in Figure 15 occur rapidly, but don't seem to limit the proposed methodology.

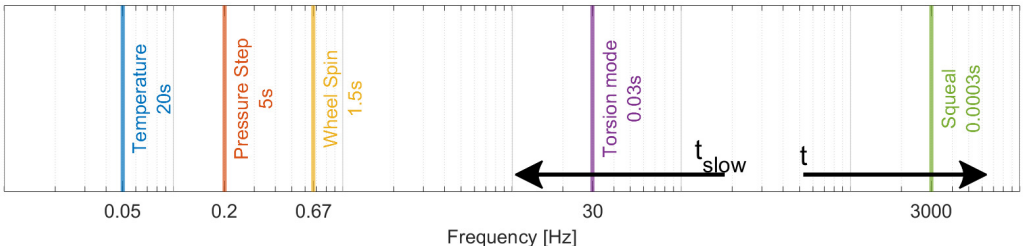

Fig. 3: Fast and slow time scales with different characteristic frequencies for test shown in Figure 2.

The name HBV emphasizes the vector nature (multiple sensors/DOF) and the relation to the harmonic balance method. These features make it different from traditional analytic signal descriptions, even though this work was clearly motivated by the Hilbert Vibration Decomposition (HVD) [16], which cleanly discusses time-scales of frequency and amplitude modulation.

When considering a time response, it is relevant to split the signal as

$$\{q(t)\} = q_{HBV}\left(\omega(t_{slow}), q_h(t_{slow})\right) + q_{Broad}(t) \tag{3}$$

a harmonic contribution given by (2) and a wide frequency contribution $q_{Broad}(t)$. In the case of brake tests, this harmonic content is linked to squeal instabilities, while the broad contribution is due to the passage of asperities under the pad which generates broadband impulse responses. In the case of simulations [5, 25], the broad contribution corresponds to transients and possibly asperities.

Figure 4 shows the spectrogram of a squeal response. Up to 14 s, the full response is shown. It is dominated by harmonics, but also contains a $q_{Broad}(t)$ contribution in the form of random noise. Between 14 and 17s, the spectrogram of the estimated q_{HBV} is shown with black lines indicating the instantaneous frequency $\omega(t_{slow})$. The presence of vertical bands is due to the time varying nature of the response.

In the 17 to 20s range, the spectrogram of $q_{Broad}(t)$ is shown. The blue bands close to the estimated q_{HBV} harmonics show that the estimation process seeks to reproduce the signal in a limited 100 Hz band. In the time

response in Figure 4 right, $q_{Broad}(t)$ is shown as a red line. Its small amplitude indicates that the estimation using 3 harmonics is sufficient.

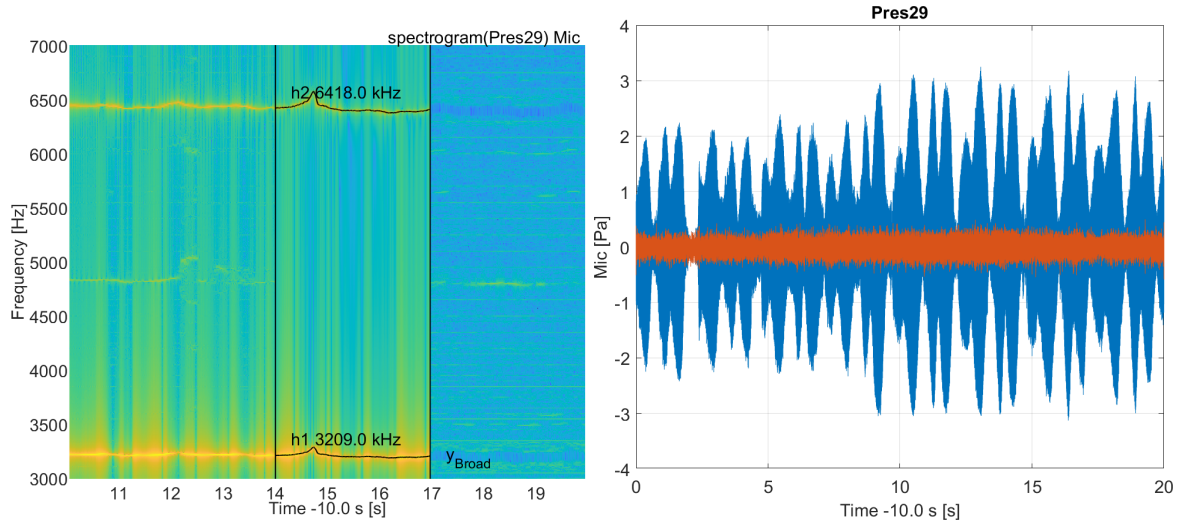

Fig. 4: Sample test of a real brake with limit cycles varying with applied pressure. Left: spectrogram with full signal [10-14s], estimated HBV signal [14-17s], broadband residual signal [17-20s]. Right: overlay of initial microphone signal $y(t)$ in blue and residual $y_{Broad}(t)$ in red.

The proposed estimation process considers the following phases :

- initial scalar estimation of analytic signals associated with harmonic 1 in each measurement, discussed in section 2.2. The proposed use of demodulation only requires selection of an initial frequency band for variations by analysis of spectrograms.
- the second step is to refine the frequency that is known to be common to multiple measurement channels. Section 2.3, shows how a Singular Value Decomposition (SVD) is used to define experimental principal coordinates and use the first one to define a unique phase.
- having an estimated phase, the amplitudes are reestimated considering a smaller capture band corresponding to the physical extent of the limit cycle content.

For the shortened automated test matrix considered here, acquisition is done at 40960 kHz, thus 24 channels stored using single precision correspond to 225 MB/mn. The complete test campaign considered corresponds to 300 GB which becomes impractical for standard PC available to test groups. Going through the demodulation process, it is possible to use the slowly varying assumption to decimate results (a fairly detailed 1 kHz was retained here although 300 Hz or 10 times the drive torsion mode period is certainly sufficient). It is also possible to reduce the number of significant digits as oscillations are now only contained in the instantaneous phase information. Data decimation by a factor 100 is thus achieved in practice and this makes it practical to implement interactive viewing of large parts of a campaign.

2.2 Estimation of scalar amplitudes using synchronous demodulation

To initialize and later refine the HBV estimation, it is proposed to simply use the well known synchronous demodulation procedure [16, 18] illustrated in Figure 5. This choice is shared with non-linear testing methodologies [17, 19, 20, 26] that use phase locked loops to track the limit cycle phase, with the notable importance of considering a vector signal as will be detailed in section 2.3.

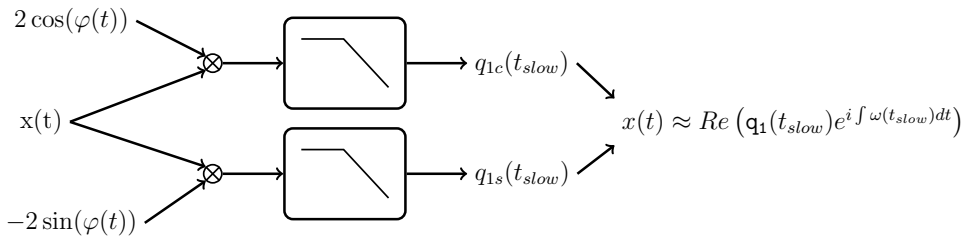

Fig. 5: Synchronous demodulation algorithm

To understand the effect of demodulation, one considers a simple single harmonic signal of the form

$$x(q_1(t_{slow}),t) = Re(q_1(t_{slow})e^{i\omega(t_{slow})t}) = Re\left((q_{1c}+iq_{1s})e^{i\omega t}\right) = q_{1c}\cos(\omega t) - q_{1s}\sin(\omega t) \tag{4}$$

where the dependence of q_{1c}, q_{1s} on t_{slow} will be dropped to alleviate notations. For a constant frequency, $\varphi = \omega t$, the product of the signal $x(t)$ with quadrature signals $2\cos(\varphi)$ and $-2\sin(\varphi)$ is

$$\begin{aligned} 2x(t)\cos(\omega t) &= 2\left(q_{1c}\cos(\omega t) - q_{1s}\sin(\omega t)\right)\cos(\omega t) = q_{1c} - q_{1s}\sin(2\omega t) + q_{1c}\cos(2\omega t) \\ -2x(t)\sin(\omega t) &= -2\left(q_{1c}\cos(\omega t) - q_{1s}\sin(\omega t)\right)\sin(\omega t) = q_{1s} - q_{1s}\cos(2\omega t) - q_{1c}\sin(2\omega t) \end{aligned} \tag{5}$$

Passing these signals in a low pass filter to eliminate the 2ω frequency component, one obtains estimates of q_{1c} and q_{1s}.

Classical constraints apply to the demodulation low pass filter. Bandwidth corresponds to the band in which one seeks to reproduce the harmonic signal (in Figure 4 the blue band in the $q_{broad}(t)$ is 100 Hz wide because a 100 Hz low pass frequency was used). If another harmonic component is present within this band, the result is unclear and methodologies discussed in the HVD developments [16, 21] should be adapted.

Forward/backward filtering should be applied to obtain zero phase filtering when possible. This is in particular used here for *a posteriori* analysis of long squeal transients (> 1 s), but not for analysis of short transients obtained when scanning the brake with a 3D vibrometer (10 to 30 ms). Filter order can be set to a high value to diminish the level of oscillations in the estimate.

Since demodulation requires an assumed phase $\varphi(t)$, it is initialized by taking a peak in a few spectrogram lines and keeping the associated frequency constant $\omega_0(t_{slow}) = \omega_{peak}$. When parameters change, the limit cycle frequency is expected to change, as visible in Figure 4 and using a constant demodulation requires that the capture band be larger than the physical frequency shift. A second step is thus needed to estimate a unique HBV frequency.

2.3 Estimation of a unique HBV frequency

Choosing a start value for the phase, typically $\omega_0(t_{slow}) = \omega_{peak}$, and $\varphi_0(t) = \omega_0 t$, enables the initial estimation of harmonic scalar signals by demodulation. Classical analytic signal theory uses a scalar signal and defines a phase correction $\varphi(t) = \varphi_0(t) + \int \delta\omega(t)dt = \varphi_0(t) + \delta\varphi(t)$ with

$$\delta\varphi(t) = tan^{-1}\left(\frac{q^0_{1s}(t)}{q^0_{1c}(t)}\right) = \int(\delta\omega dt). \tag{6}$$

In other words, phase evolution of harmonic 1 signal $q^0_1 = q^0_{1c} + iq^0_{1s}$ is interpreted as an error on the frequency estimate to be corrected to achieve constant phase.

This does not account for the HBV signal model (2) constraint that the frequency is common to all spatial components and that the shape is a complex vector $\{q_h\}(t_{slow})$. Thus rather than selecting a single sensor as reference, which was found to be unreliable, it is proposed to correct the HBV frequency by seeking to have a principal coordinate close to zero phase.

A principal signal and the associated coordinates is obtained by computing the Singular Value Decomposition (SVD) of the demodulated harmonic $h = 1$ signals $q^0_1(t_{slow}) = q^0_{1c}(t_{slow}) + iq^0_{1s}(t_{slow})$ at N_S sensors and for N_T time steps. To further achieve the use of a real vector with a complex amplitude, as when combining sequential limit cycle tests [27], the real and imaginary parts are reordered sequentially to obtain real valued left principal vectors $\{u_j\}$ in the following decomposition

$$\left[q_{1c}(t_{slow}) \quad q_{1s}(t_{slow})\right]_{N_S\times(2N_T)} = \sum_j \{u_j\}_{N_S\times 1}\left(\sigma_j\left\{v^H_{jc} \quad v^H_{js}\right\}\right)_{1\times 2N_T} = \left[u_j\right]\left\{q_{1c,j}(t_{slow})\ q_{1s,j}(t_{slow})\right\} \tag{7}$$

resulting in $\{u_j\}$ principal shapes defined at sensors and, for each principal shape j, a generalized amplitude vector $\{q_{1c,j}(t_{slow})\ q_{1s,j}(t_{slow})\}$, function of time, that is approriately reordered as a complex generalized amplitude function of time

$$q_{1R,j}(t_{slow}) = q_{1c,j}(t_{slow}) + iq_{1s,j}(t_{slow}) \tag{8}$$

where the R index is used to indicate the fact that this corresponds to a reduction of the signal dimension. Note that the names reduced and principal are used interchangeably by different communities.

The SVD gives an ordered set of principal amplitudes, since the singular values σ_j are positive real with decreasing amplitude for increasing j. If the response is dominated by two singular components, the whole test interval is properly described by a single complex shape. If a few more are needed, this may be an indication that the harmonic 1 shape q_1 does not simply come from the combination of two real shapes. In Figure 6, the first two principal coordinates dominate when the amplitude is large (as expected from the SVD), but a third component, shown in grey, has notable contributions in the lower amplitude regimes when $q_{1R,2}$ is below 10g. Note that the use of principal coordinates is clearly linked to the notion of modal filters used in [18] for example.

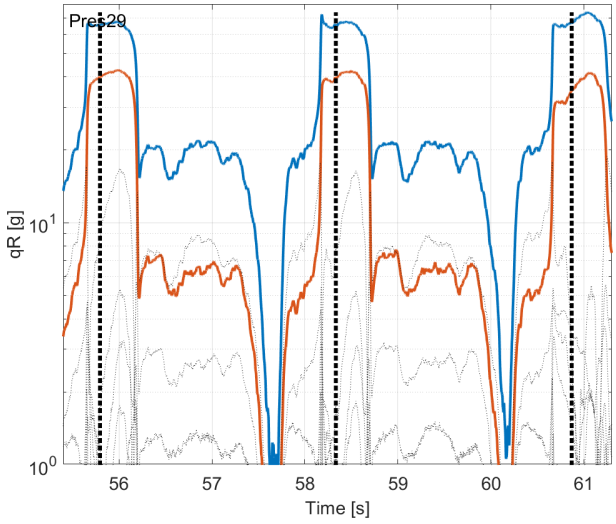

Fig. 6: Principal amplitudes during three intermittent squeal occurrences. $q_{1R,1}$ in blue, $q_{1R,2}$ in red, the following in gray. Vertical lines indicate a complete wheel revolution.

As mentionned in the motivation, the HBV frequency is corrected by seeking to have the first principal coordinate $q_{1R,1}(t_{slow})$ close to zero phase. Note that in $1R,1$ the second 1 refers to the first principal coordinate (indicated by the R for reduced), while the first 1 to the fact that this has been applied to the first harmonic (although using higher harmonics might clearly improve frequency estimation accuracy). The instantaneous frequency correction (and not phase correction shown in (6)) is then given by

$$\delta\omega(t_{slow}) \approx LP\left(\frac{1}{dt}tan^{-1}\left(\frac{q^0_{1R,1}(t_{n+1})}{q^0_{1R,1}(t_n)}\right)\right) \tag{9}$$

Using a ratio of succesive samples $q^0_{1R,1}(t_{n+1})/q^0_{1R,1}(t_n)$ provides a phase increment. As suggested in [16], this avoids phase wrapping issues since increments are small.

The division by dt gives a frequency correction that forces q_{1R} to be exactly real and an updated instantaneous frequency given by $\omega_1(t_{slow}) = \omega_0(t_{slow}) + \delta\omega(t_{slow})$. The zero phase constraint is not inherent to the harmonic balance methodology, so that it is preferred here to enforce the constraint that ω is expected to be a function of t_{slow} by applying a Low Pass (LP) filter, set with a cutoff frequency based on frequency content considerations shown in Figure 3. Later integration then recovers the phase correction (6).

As an illustration, one will consider a measurement with multiple accelerometers. As shown in Figure 6, amplitudes tend to vary notably.

Figure 7 left is a zoom on a high amplitude area. The raw estimate of individual sensors, between grey dotted line, is relatively consistent, but the estimate based on the principal coordinate (unfiltered in dashed red and filtered in solid

red) has been found to give reliably consistent estimates. In the right plot, a low amplitude area is chosen. Individual sensors give very noisy estimates, but the principal coordinate gives a proper result. The use of principal coordinates (the vector nature of the HBV signal), thus gives access to much lower amplitude parts of the test, which is helpful to bridge the gap between low amplitude complex modes and high amplitude limit cycles.

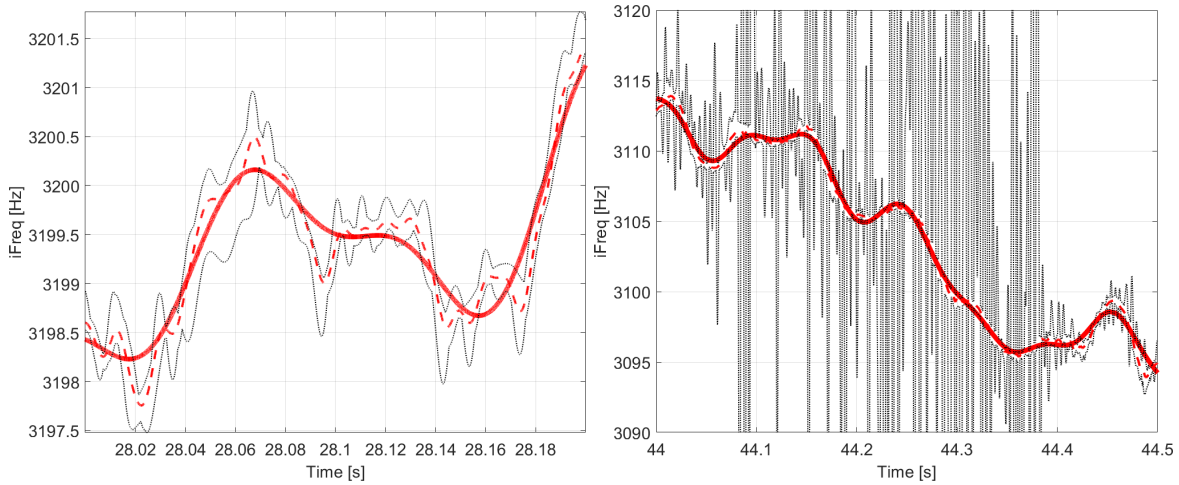

Fig. 7: Estimated frequency error. Bounds on individual sensors shown in grey. Filtered correction (9) in solid red. Without lowpass in dashed red. Left: high amplitude area. Right: low amplitude area.

The use of the largest number of sensors for the principal coordinate computation gives the best result unless some of those have problems. In the present test, saturation of the IEPE circuits led to some wrong measurements, which clearly bias the instantaneous frequency estimation, and were thus discarded.

The corrected instantaneous frequency $\omega_1(t_{slow}) = \omega_0(t_{slow}) + \delta\omega_0(t_{slow})$, could be used to update the estimate by correcting its phase $q_1^1 = q_1^0 e^{i\int(\delta\omega_0 dt)}$, but the choice made here was to iterate once by restarting the demodulation procedure using the updated instantaneous frequency in other words get $q_1^1 = \text{demod}(q(t), \omega_1(t_{slow}))$. This shape estimation phase might not be necessary, but the cost is small.

When tracking large frequency ranges (as in the parametric test of section 3.4), the bandwidth of the first demodulation must be larger than the total frequency excursion (about 300 Hz in the case of section 3.4). But at any instant the limit cycle content is actually narrower, so that a lower band is more desirable (100 Hz was used). Of course an initialization based on a few spectrogram lines might be more adapted than the constant choose for initialization. Another question left open is the convergence of this multistep algorithm towards a fixed point.

It is finally worth mentioning computing the SVD is not compatible with real time applications, but weighting individual phase corrections by the amplitude of each sensor achieved similar results. This is similar to modal filtering, which can be used in real time [18].

3 Squeal illustrations

3.1 Test configuration and experiments

The full brake shown in figure 1 is mounted on a dyno test bench which imposes the disc rotation through a shaft transmitting the torque. The system is equipped with 17 accelerometers, 1 microphone and 6 sensors measuring the following brake environment parameters: brake pressure, wheel speed, friction pad temperature, torque and disk/bracket distance The accelerometer positions are shown in Figure 1 right. The caliper is equipped with 2 tri-axes accelerometers at the top of each "finger" in contact with the top pad, two accelerometers at the bottom of caliper pins and one below the piston chamber. Each side of the bracket is equipped with two accelerometers close to the top and bottom on the pinholes and one close to the attachment with the knuckle. Three accelerometers are finally placed on the knuckle.

To ensure that the proposed methodologies are compatible with industrial-scale measurements, a small certification experiment was designed with the following braking events:

- 40x Drag events: Constant brake pressure (12-18 bar) at constant speed (2-10 km/h)

- 40x Pressure stops: Stop from initial speed (15-30 km/m) at constant pressure (12-18 bar)
- 40x Deceleration stops: Stop from initial speed (15-30 km/h) at constant deceleration (1-3 m/s²)
- 40x Pressure rampings: Linear increase-decrease in pressure (12-18 bar) at constant speed (2-10 km/h)

For each type of brake event, the corresponding parameters are randomly chosen in the parameter ranges (which have been defined with the brake manufacturer to focus on specific braking conditions). A temperature range (40-100 ℃) is also imposed using a thermocouple placed in the friction pad below the pad backplate. Because temperature cannot be controlled while braking, this temperature corresponds to the one at the beginning of braking events: it is managed by heating (braking) or cooling (waiting or air-cooling)between braking events. These 160 brake events resulted in 20 minutes of recorded time data sampled at 40 960Hz, representing 10 GB.

The small certification experiment is used in sections 3.2 to demonstrate applicability to general tests. In section 3.3 a specific test is used to focus on the intermittent squeal occurrences and their relation with parametric root locus. Section 3.4 then focuses on parametric testing using slow variations of pressure. Finally, section 3.5 discusses steps taken when coupling test and FEM results.

Note that temperature is measured with a single thermocouple placed in the pad friction below the pad backplate whereas a temperature gradient is expected, with the highest temperature close to the sliding contact. Precisely taking into account the effect of temperature is out of the scope of this paper, and would probably require additional information such as measuring the temperature gradient with a thermal camera. The current single temperature point is a first step to take into account thermal influence and is a hint to avoid misinterpreting limit cycle parameter dispersion that would appear purely random without it.

3.2 Classification of occurrences using features and parameters

Brake characterization is performed using a wide test matrix covering a range of operating parameters. Figure 8 illustrates a sample 20 mn test matrix (real ones are often notably longer). Epistemic controlled parameters are pressure, wheel speed. Epistemic measured parameters are temperature, relative disk/bracket position, torque, ... A test matrix is usually defined by those parameters and shown in plots such as Figure 8 left. Position of the wheel is often considered random as it is typically ignored in computations, but it was here estimated by integration of the wheel speed and will be shown in section 3.3 to have a major effect on intermittent squeal (integration however does not provide a clean way to really position the disk). Pad wear is another parameter known to have a clear effect.

Features first considered are high amplitude occurrences shown in a spectrogram. Distinction between acoustic and vibration amplitude is useful to answer distinct questions : is noise going to be considered an end user quality issue? Is vibration indicating the proximity to an instability area? When an occurrence area is identified, the next issue is to diagnose its extent.

Classification seeks to group similar squeal occurrences. Similarity is judged by output features: limit cycle frequency, amplitude and shape, but also by input parameter. Epistemic input parameters are associated with time scales shown in Figure 3, which indicates that one needs to at least consider fractions of a wheel turn (20 Hz) or even fractions of a drive torsion period (300 Hz to have 10 points per period). Unmeasured parameters such as the pressure distribution field, can be considered random even though they are correlated to measurements such as the torque (see Figure 15).

The test matrix analyzed in this section contains 24 channels, discussed in section 3.1. Sampling at 40kHz with 32bits generates 220 MB/mn of data throughput. The HBV signal model estimation allows data size reduction: the slow time variations allow sampling at 1kHz and data throughput drops to 5.5 MB/mn, interest on high values would also allow reduction of the number of significant bits. Nevertheless, the end data set is still more than a million points and navigation is thus critical. Using the mean pressure/temperature over each wheel turn as shown in Figure 8 left is often used in industry. The parallel coordinate plot shown in Figure 8 right is another classical tool used help navigation and visual detection of correlations.

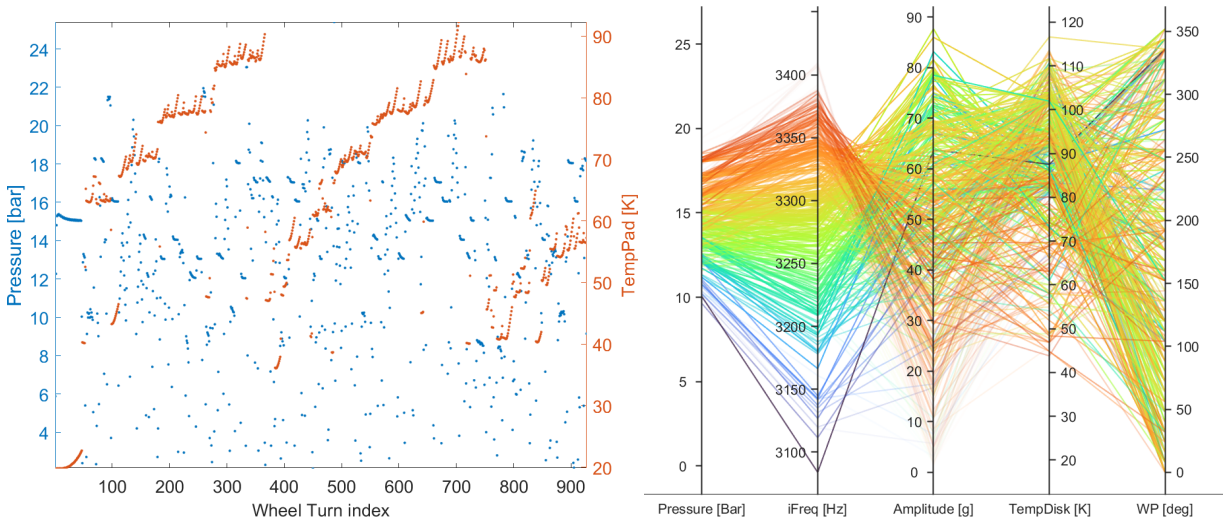

Fig. 8: Left: pressure and temperature for 350 time segments corresponding to wheel turns. Right: parallel coordinate plot associated with the test matrix.

With so much data, efficient characterization must rely on classification techniques. Aggregating operational points into clusters with comparable features gives a synthetic view of the overall sensitivity and parametric regression by groups [28]. The most common clustering for squeal is to build cluster with high amplitudes at similar frequencies. Figure 9 left shows the maximum microphone and vibration amplitudes from two spectrograms. It shows that the classification may not be trivial. Occurrence `OccA` spreads between 3.1 and 3.4 kHz depending on the operating condition. It has strong levels of harmonics labeled h2 and h3 in Figure 9. Occurrence `OccB` in between 4.7 and 5.2 kHz, is only visible in the vibration amplitudes and only during 30 s out of 1200 in the test. Occurrence `OccC` in the 10.6 to 10.8 kHz range has the highest level, but is associated with short intermittence (33s spent above 10% of maximum level).

Further refinement of sensitivities can be performed trying to highlight trends. The 2D histogram shown in 9 right, uses the demodulation result and corresponds to a cumulative amplitude ($a_p(pixel) = \sum_{t\in \text{pixel}} a(t)dt$) associated with frequency and pressure bands shown as pixels. Transparency is set to $a_p(pixel)^{0.2}$ to highlight the area in poor contrast displays, but furtherwork on this integral criterion is clearly needed. Occurrence frequency increase with pressure is the first order trend. The spread of frequencies at a given pressure corresponds to the effect of other parameters and need further analysis. One can see multiple horizontal lines at 12, 13, ... 18 bars. They result from drag experiments, where pressure is kept constant for a long time and thus should be seen as a bias for the interpretation of results. Finally, it is unclear whether there is a separation between the lower left corner (<3200 Hz, <11.3 bar) and the rest of the responses. Answering this will require using shapes for clustering efforts.

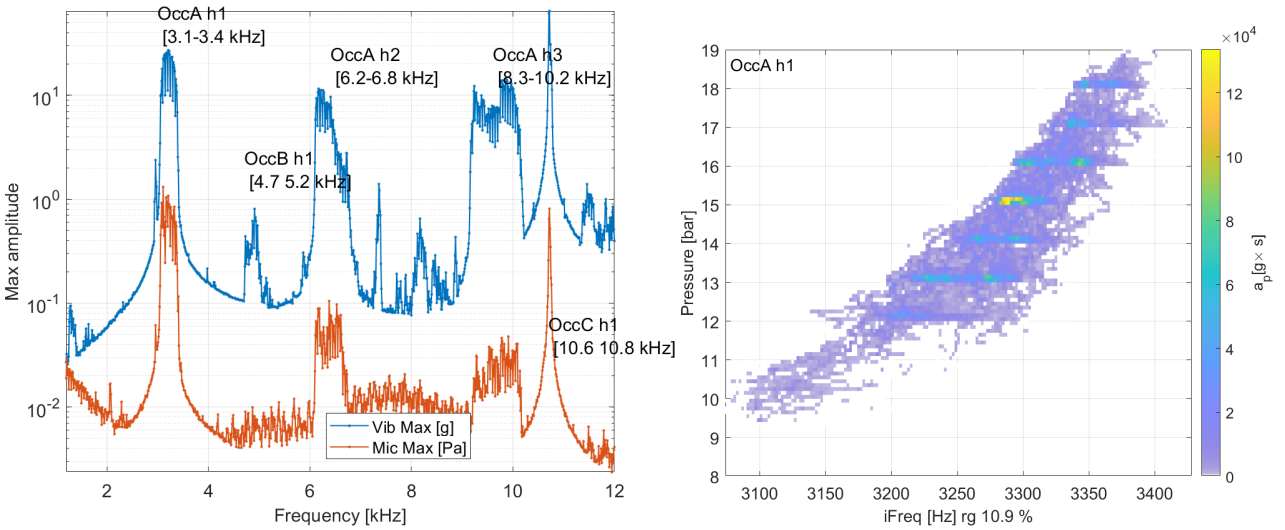

Fig. 9: Left: maximum amplitudes on microphone and vibration. Right: histogram of instantaneous frequency and amplitude `OccAh1`.

Histograms of other occurences are illustrated in figure 10. The differences between `OccAh1` and `OccAh2` show that the relative amplitudes of harmonics evolves with pressure, but detailing the trend is beyond the scope of this paper. For `OccBh1` the sensivity to pressure is smaller and the number of occurences is much smaller (this would be qualified as rarely occuring). For `OccCh1` the frequency is mostly insensitive to pressure.

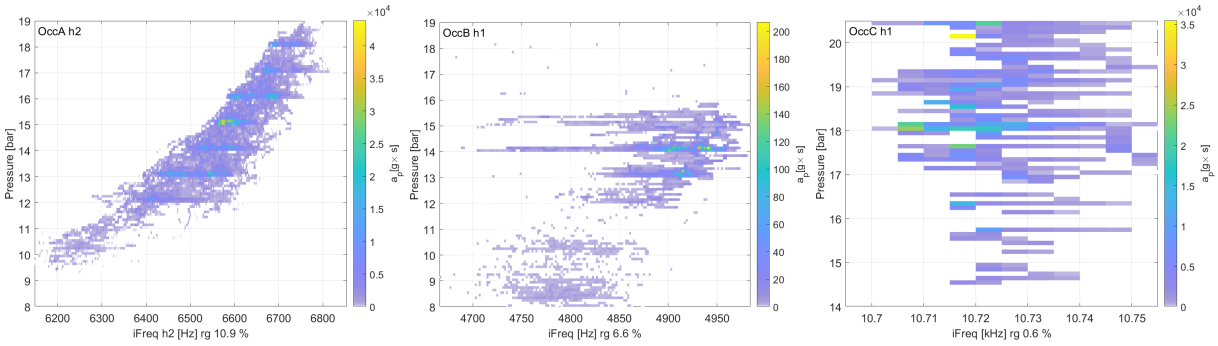

Fig. 10: Histograms of instantaneous frequency and amplitude. Left: `OccAh2` harmonic. Center : `OccBh1`. Right : `OccCh1`

Using HBV estimates of the harmonic 1 shapes, a first empirical shape clustering technique is illustrated in Figure 11. The instant t_i with the highest vibration amplitude is chosen as reference. Instants whose shape has a correlation by the MAC (Modal Assurance Criterion)

$$MAC(\{q_r(t)\}, \{q_r(t_i)\}) = \frac{\left|\{q_r(t)\}^H \{q_r(t_i)\}\right|^2}{\{q_r(t)\}^H \{q_r(t)\} \{q_r(t_i)\}^H \{q_r(t_i)\}} \tag{10}$$

above a given threshold (0.8 here) are considered within the same cluster. The process is repeated until new clusters have too few points (here 500 out of 1.6e6). The point used as reference for each cluster is marked by a ci (it does not correspond to a cluster centroid). The first cluster $c1$, in blue in Figure 11 left, corresponds to instant frequencies in the 3200 to 3400 Hz range. This shape rarely corresponds to low amplitudes. The transition between low and high amplitudes is seen as a yellow cluster $c3$. For test/analysis correlation this means that computations, based on complex eigenvalue analysis of a system linearized around the static sliding state, would correspond to the yellow cluster. Then, as amplitude increases, limit cycles would come close to the blue cluster.

The second cluster $c2$ corresponds to occurrences between 3080 and 3160 Hz. It is separate from the blue cluster and most transitions occur with amplitude raising from zero (intermittent squeal), even if some happen as transitions

between the two limit cycles. The two shape clusters thus confirm the intuition from Figure 9 right (histogram analysis): two different mode couplings occur below and above 11 bar, resulting in two different shapes.

It is important to note that the use of thresholds hides the fact that transitions occur smoothly. As modal combinations evolve with parameters, it is more relevant to use a norm measuring the distance between shapes, such as expansion based mechanical deviation energy [27], or more simply by considering the angle between the subspaces spanned by each complex shape [29]. Taking the dimension two real subspaces associated with $\left[Re(q_1(t)) \quad Im(q_1(t))\right]$, one computes the subspace angle with respect to the subspace at maximum amplitude (point labeled $c1$). Figure 11 right illustrates that the evolution of shapes is notably dependent on frequency and amplitude. Compared to the subspace of the higher amplitude points noted $c1$ in the Figure 11, the angle clearly increases, implying that the shapes evolve, as the operating condition changes. Note that subspace angles are classically used in the k-means clustering technique with additional strategies to choose the center point [30].

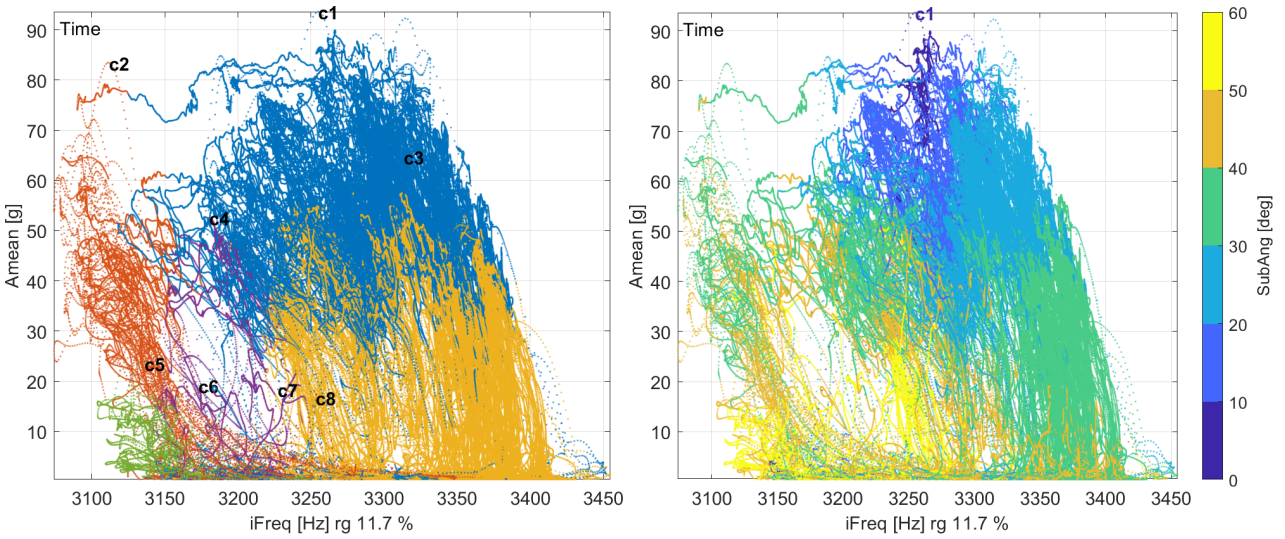

Fig. 11: Frequency vibration amplitude map for the limit cycle in the 3080 to 3450 Hz range (Amean is taken to be $||q_1(t_{slow})||$, the 11.7% corresponds to the relative width of the frequency window, which is a useful indicator of sensitivity). Left: clustering as MAC<0.8 boundaries. Right: color indicating subspace angle to point `c1`.

Figure 11 highlights a clear correlation between frequency and amplitude/shape evolution. The next section will seek to draw a parallel, with classical control theory where the evolution of poles and complex modes with parameters leads to a root locus.

3.3 Transient root locus: using numerical insight for experimental analysis

The literature on non-linear vibration often highlights that vibration amplitudes play a critical role and can be usefully considered as an environmental parameter characterizing how the system behaves [31]. The Hoffman model is a well known phenomenological model of squeal [32], where a varying parameter, the friction coefficient, induces evolution of poles both in terms of frequency and damping.

A variant of this functional model has been detailed in [33]. The main change is the consideration of a non-linear contact stiffness leading to an operation point that depends on static pressure and dynamic pressure fluctuations. Introducing a sensitivity to applied pressure is thought to be more representative of the present situation illustrated by Figure 9 right. Note that the model has been tuned to obtain limit cycles representative of brake squeal, but is not a model corresponding to the experimental configuration illustrated in this paper. The following simulation results are not to be compared directly with previous experimental results, but only illustrate the trends and provide clues for deeper analysis of tests.

The left view of Figure 12 shows frequencies as a function of pressure. But the only area measurable with squeal occurrence tests is the unstable zone and its edges, which can be seen in test as stable/unstable transitions. The right view emphasizes another key aspect of parametric coupling of modes : the frequency and damping ratio evolve simultaneously. This corresponds to root locus analysis, a classic notion of control theory, where system transition

from stable to unstable by mode lock-in typically occurs with a real and imaginary parts of poles, as well as mode shape depending on a gain parameter.

A classical property of HBM solutions is that a non-linear relation between gap and pressure in the contact area will generate a nonlinear coupling between harmonics 0 and 1 of gap (static penetration and vibration amplitude), and harmonics 0 and 1 for pressure (static and harmonic 1 pressure). This non-linear relation can be seen as an amplitude and pressure dependent equivalent stiffness [33]. In Figure 12, one thus varies a contact stiffness parameter that leads to the modal interaction where frequencies, damping, and shapes evolve. In transients, one expects, and finds numerically, convergence to the stability edges, corresponding to points L2 and R2 of Figure 12 right in this simple case.

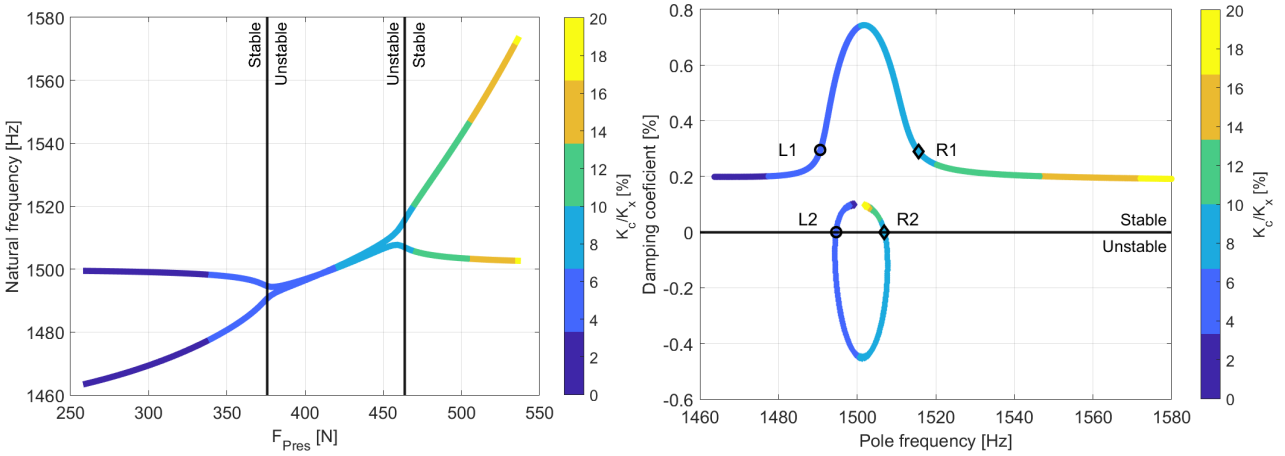

Fig. 12: Evolution of the linearized system poles as a function of the static load F_{pres}. Left: natural frequency. Right: root locus (damping as a function of frequency) for the same variation. Color giving a ratio of contact stiffness to horizontal stiffness [33].

To confirm that this expected trend is measurable in tests, one considers a brake event leading to squeal occurrence measured close to 18 bars and classified into OccCh1 in Figure 9 left. This brake event has been chosen over other occurence frequencies because squeal is intermittent: in a short time period, system switches between stability and instability, and a high range of amplitude growth/decay is covered. In the functional model, intermittent squeal corresponds to crossing of the stability boundary due to parameter changes, illustrated by the black lines in Figure 12. The short length of occurrences makes the analysis using a spectrogram such as shown in Figure 13 left quite sensitive to parameter choices (buffer length, overlap, window, ...). Using the HBV estimation, the HBV signal model makes it easier to see in Figure 13 right that each occurrence happens with a coupling of frequency decrease for growing amplitude followed by a smaller frequency increase for decaying amplitude.

In the Linear Time Invariant (LTI) complex mode analysis, a pole λ is used to explain growth/decay events with, for lightly damped poles, slow time amplitude varying with $exp\left(Re\left(\lambda\right)t\right)$. For growth phases, the real part of the pole is positive, for decay phases it is negative. Using an amplitude estimate $A(t_{slow})$, the principal coordinate (8) or the norm of the HBV vector, one thus defines a decay ratio using

$$\{\zeta_D(t)\} = -\frac{1}{\omega(t_{slow})}\frac{\partial log(A(t_{slow}))}{\partial t} \tag{11}$$

which would correspond to the damping ratio in the case of a single degree of freedom system. Note that this inspired by the classical logarithmic decrement method and work done on damping in bolted joints [24].

Growth phases are thus associated with a negative decay ratio, as a negative damping ratio describes an unstable LTI system. The values in the $[-0.12\ 0.06]\%$ range are related to the frequency range of 0.6% as in root locus analysis evolution of real and imaginary parts of the poles have similar amplitudes. The decay ratio evolution is strongly correlated with a frequency evolution which corresponds to the expected behavior in the functional model of Figure 12 right.

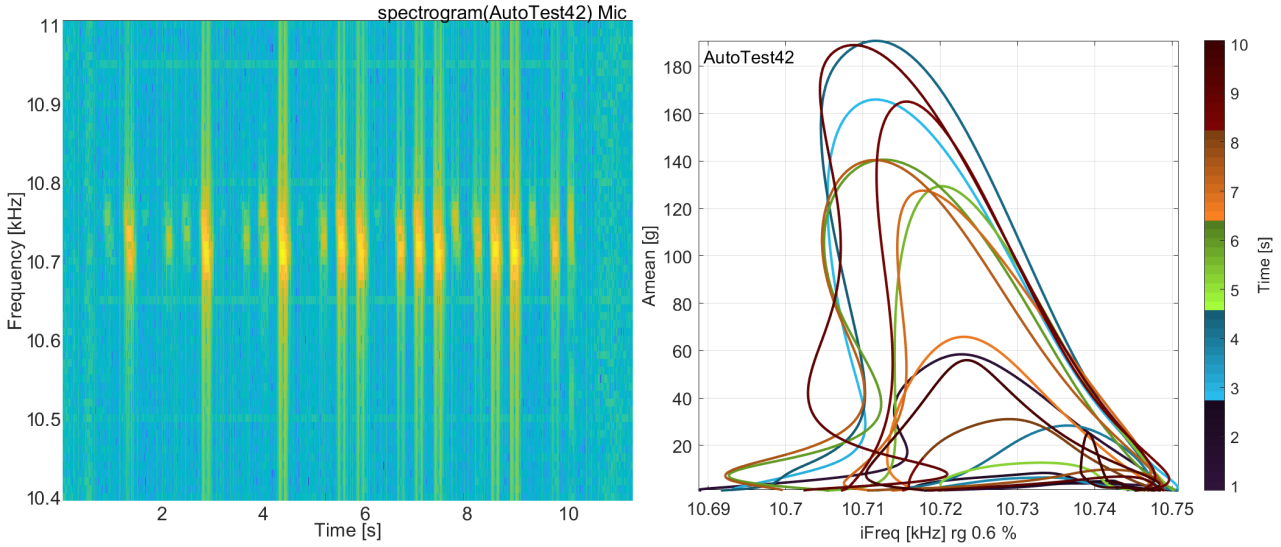

Fig. 13: Left: spectrogram illustrating the intermittent squeal. Right: amplitude evolution as a function of frequency.

In the simple functional model, all changes are represented by the scalar pressure parameter, but many other parameters are involved in the operating conditions of the measured brake system. To understand the physical mechanism leading to intermittent squeal in the real measurements, Figure 14 focuses on the disk (or wheel) position (WP) associated with squeal occurrences. Figure 14 left shows that repetitions correspond to different parts (each color being associated with a different quadrant). In Figure 14 right, the decay ratio is shown on a spiral of radius growing with time. It thus appears that the growth/decay events are consistently positioned in space for multiple wheel turns.

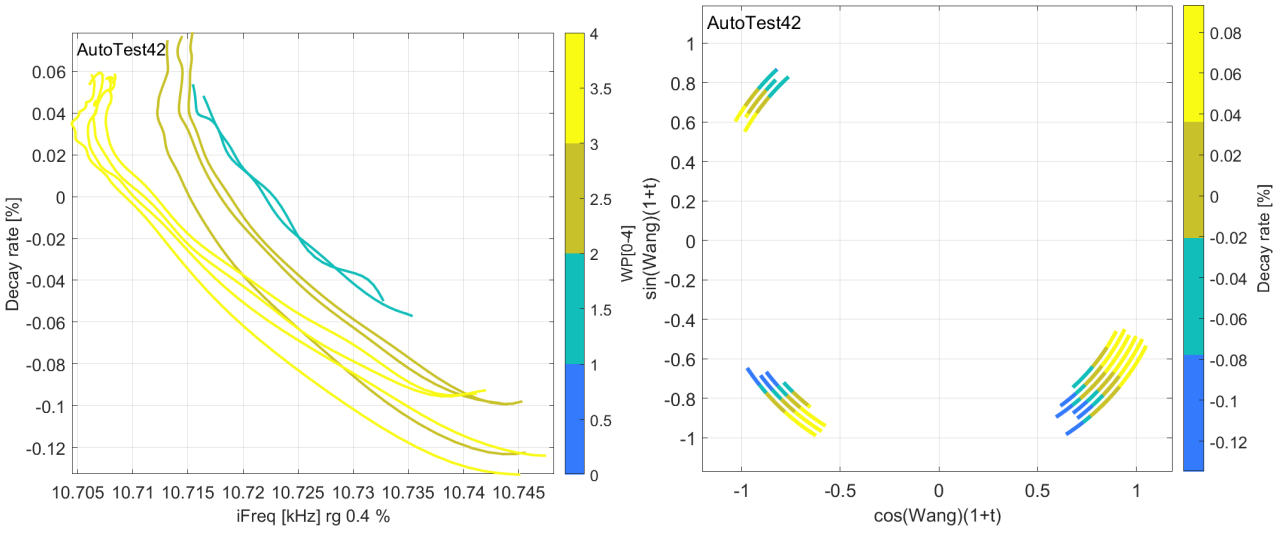

Fig. 14: Left: decay ratio as function of frequency (color indicates wheel angle). Right: decay ratio shown as color positioned on a spiral to emphasize the angular repetability.

Figure 15 left focuses on a displacement sensor placed between the bracket and the disk. Although the disk was selected to be as flat as possible, one clearly sees that fluctuations of several microns occur regularly. This implies that pad pressure and pad guiding springs see varying loads. Figure 15 right further shows the measured torque. The correlation between wheel position, bracket/disk distance and torque fluctuations is very clear. This is consistent with the assumption that pressure distribution under the pad is strongly affected by the geometrical disk defects and also highlights that torque impulses are a source of broadband background noise. One can also note that although the velocity is maintained constant, the torque is diminishing over the 10 seconds of the experiment (as shown by the time

labels in the Figure 15).

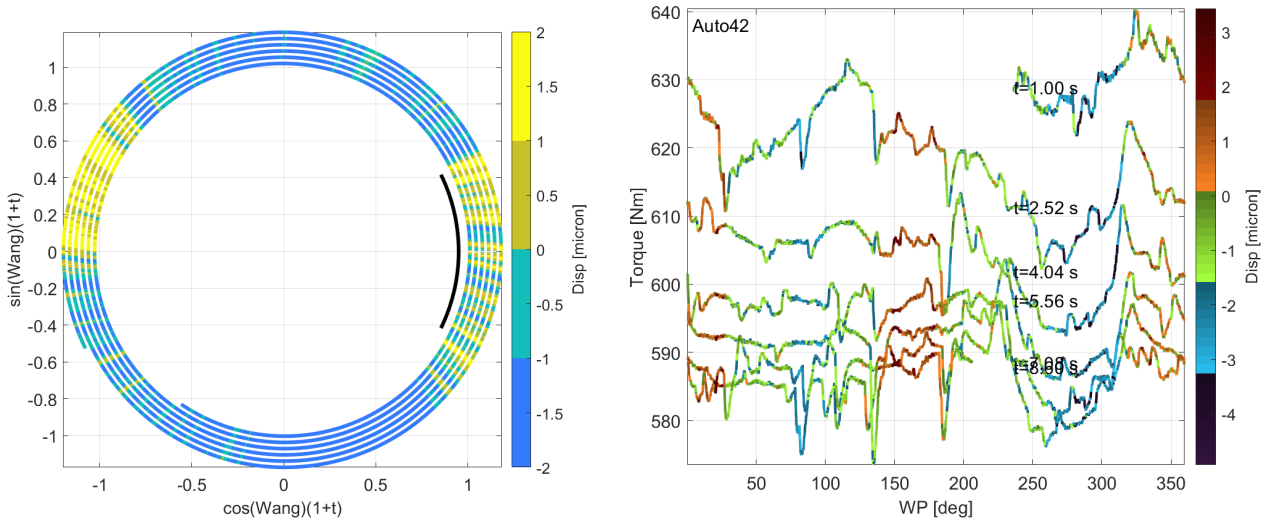

Fig. 15: Left: disk/bracket distance shown as color on a spiral (black line is an indication of pad extent). Right: torque as a function of wheel position (WP), distance (Disp) shown as color. Time labels show slow decrease of torque during the test, each line corresponding to a complete revolution.

3.4 Parametric testing and clustering of occurrences

Operating at a fixed condition in speed/pressure does not give a good understanding of the stability boundary. It is thus desirable to analyze experiments where parameters are varied. Such variation can be motivated by physical operating conditions (the speed slows as the car stops, the pressure changes as the driver presses or releases the pedal) or simply seek to cover the parametric space. In Figure 16 pressure is varied from 15 to 10 Bar and back up with 0.5 Bar increments lasting between 2 and 9s.

Figure 16 illustrates that intermittent squeal occurs in the 14.5-15 Bar range (yellow areas in the right figure) and the 11-11.5 Bar range (lighter blue areas). These thus correspond to the edges of the parametric instability domain. The edges are not sharp as the disk is not flat which, as shown in the previous section, is sufficient to have the system transition between stable and unstable behavior. In the intermediate pressure area 11.5 to 14.5 bar, squeal is permanent but still subject to parametric variation, which can go up to being intermittently stable, associated with the wheel position.

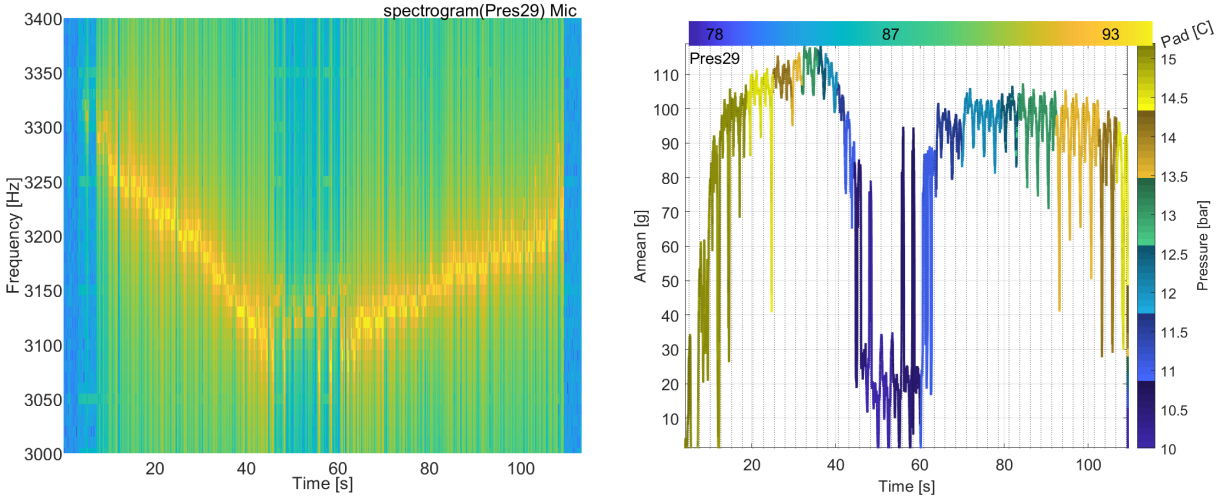

Fig. 16: Left: spectrogram of microphone measurement. Right : harmonic 1 acceleration amplitudes as a function of time, pressure as color and pad temperature shown in the upper horizontal bar (independent color scale).

Figure 17 seeks to analyze these results as an experimental root locus. In the left plot amplitude is shown as function of frequency. Intermittent squeal corresponds to areas with notable amplitude changes. In the right plot, one seeks to emphasize the relation with poles and thus displays decay ratio as a function of frequency. As before frequency and decay ratio evolve simultaneously. The stability boundary at high pressures is close to 3260 Hz, while for low pressures it is close to 3150 Hz. The transitions are also different at low and high pressure indicating that the associated mechanism has changed. The comparison with poles is imperfect as frequency, amplitude, damping and shapes are evolving simultaneously. But showing this evolution seems important to address the question of relations between limit cycles and complex modes.

During the developements, it was also realized that improper instant frequency tracking, for example using a first demodulation low pass filter set too low, generated amplitude decays linked to frequency error. Future work will thus be needed to fully control distorsions due to instant frequency estimation.

The repeatability for increasing and decreasing pressure is good but not perfect (this is very visible in the amplitude/frequency plot). This is expected as torque decreases over time (as shown in Figure 15 right), the pad temperature increases from 78 to 93 C (as shown by the upper colorbar), and pressure steps vary in length. In terms of the certification experiment of figure 9 right, this corresponds to the horizontal width of the instability area.

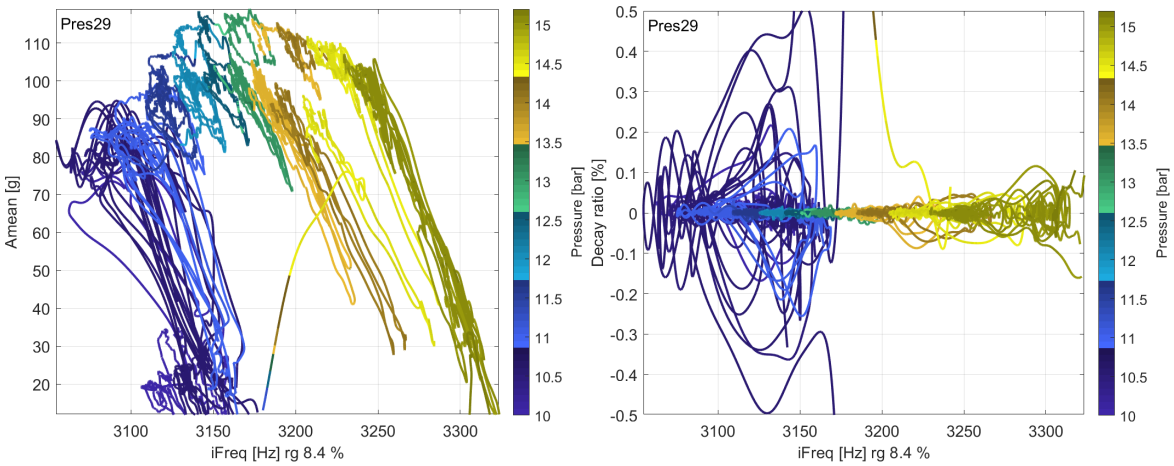

Fig. 17: Left: harmonic 1 amplitudes as a function of frequency and pressure as color. Right: decay ratio as a function of instant frequency and pressure as color (transient root locus)

When computing a root locus, it is known that interacting modes will change shape. When doing parametric computations of instabilities, it has been found useful to use clustering techniques such as the k-means to clarify parametric areas of similar behavior. Clustering as discussed in section 3.2 can be done here using the shapes defined in this case by 16 accelerometer measurements.

The resulting clusters are shown as colors in Figure 18. The highest amplitude cluster $c1$ in blue corresponds the stable limit cycle. Intermittent squeal at high pressure is cluster $c2$ close to 3100 Hz, 30-45s interval for downward pressure and 60-90s for upward pressure. Cluster $c3$ close to 3250 Hz corresponds to the other edge of the instability area.

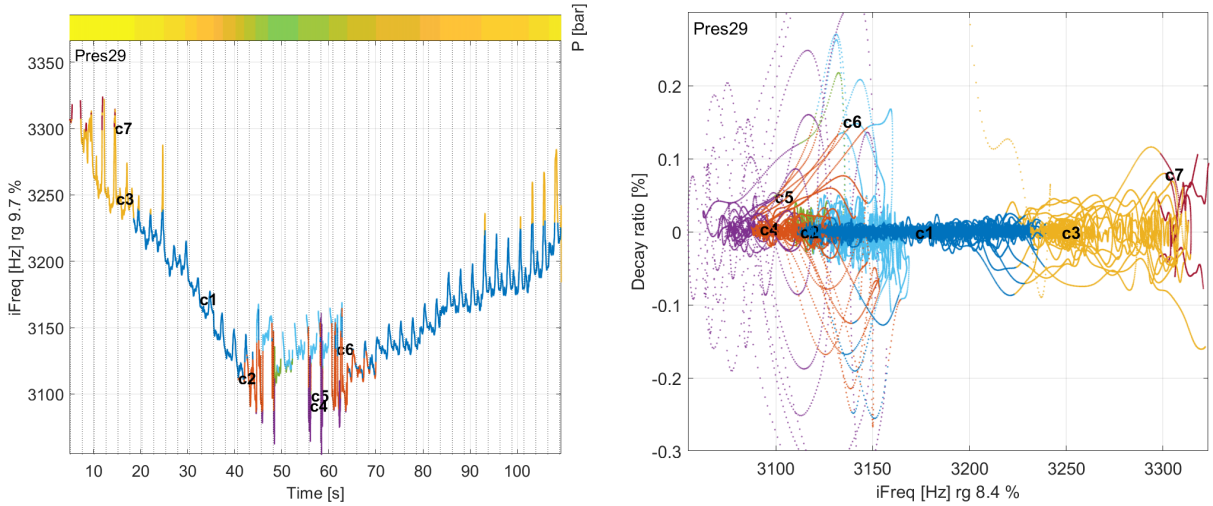

Fig. 18: Left: instantaneous frequency as a function of time, shape clusters (MAC<0.9 tolerance) as colors and pressure shown in the upper horizontal bar (independent color scale). Right: transient root locus with cluster colors.

To analyze the shape transition, the first harmonic of the HBV signal $\{q_1(t)\}$ is decomposed into j real valued principal shapes $\{u_j\}$ and their associated complex principal coordinates $q_{1R,j}(t)$ using (8). Figure 19 left shows the evolution of the principal coordinates in the time interval [9-44]s which contains 3 clusters. In the [15-40]s band, the squeal is constant, close to its highest amplitude, and it is reasonable to analyze its complex shape as a combination of the two main real shapes.

Taking the first generalized coordinate $q_{1R,1}$ as reference, Figure 19 right shows the amplitude ratio $|q_{1R,2}/q_{1R,1}|$ and the phase difference $arctan(q_{1R,2}/q_{1R,1})$ evolving with pressure – the main driver of instantaneous frequency. In the permanent squeal time window (12.5-14.5 bar pressure range), the amplitude of the second shape grows with pressure, up to becoming predominant at highest pressure. The phase difference between the two real shapes is fairly stable. At low (11-12 bar) and high (15 bar) pressure, squeal is intermittent which explains the horizontal spread in Figure 19 right. The study of these transition zones would require a more detailed analysis, as the contributions of the other shapes are no longer negligible.

The analysis of shape transitions in terms of subspace of low order is useful for both testing and test/FEM correlation. During test, it is often difficult to stay precisely at the same operating condition: uncontrolled parameters such as bracket/disc distance or temperature evolve during a 3D-SLDV scanning; several braking events may be necessary to measure batches of accelerometers. Test/FEM correlation can seek to analyze global trends (are the measured principal shapes present in the frequency band of interest in the model?) or detailed behavior (does the mode coupling evolve with parameters the same way in test and simulation?).

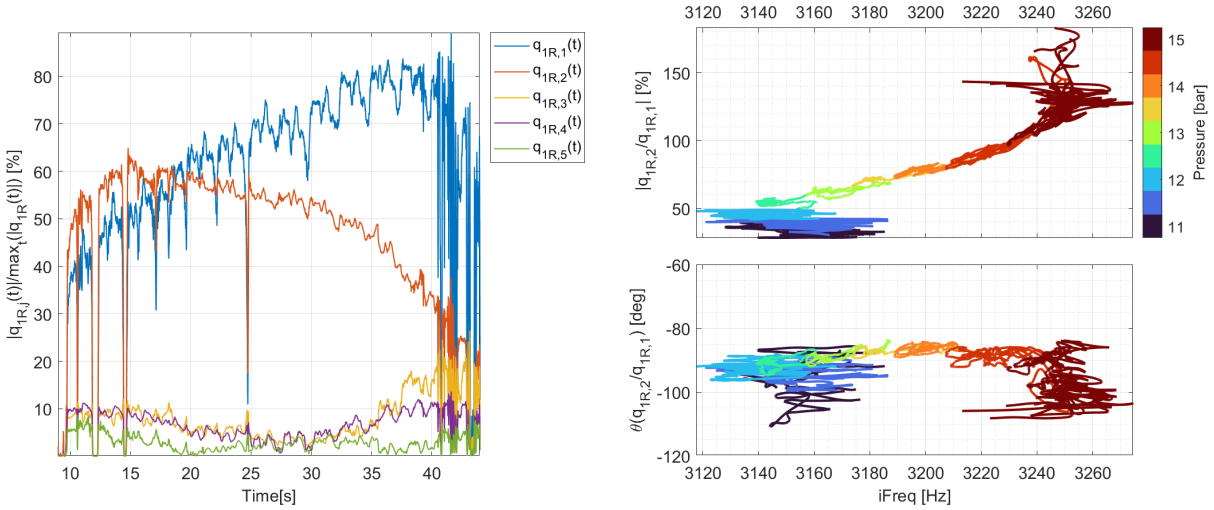

Fig. 19: Left: participation of real generalized coordinates to the complex shape for stabilized squeal [19-35]s. Right: evolution with frequency and pressure of the two first generalized coordinates (amplitude ratio and phase difference).

3.5 Towards hybrid Test/FEM models

In many cases, squeal mitigation is performed testing a range of classical counter measures : viscoelastic shims, friction cuts and chamfers, ... This however does not really use initial experimental results to guide the design process. The usual alternative is to use tests to gain an understanding of involved shapes. Figure 20 illustrates typical shapes obtained from test. Figure 20 left shows that the number of accelerometers is only sufficient to have very coarse information.

Laser vibrometer measurements are then typically used to obtain a detailed shape, as illustrated in Figure 20 center. This requires an assumption of invariant subspace at reference accelerometers to merge the batch experiments corresponding to each laser measurement. The methodology discussed in [27, 34] typically gives better results than the Polytec FastScan procedure, the latter being more adapted to time invariant cases as presented in [35].

Regarding squeal cluster analysis in Figure 11, both model and test indicate that multiple modes exist within the band of interest. Further work is needed to ensure that the measured shapes are reliably constant during the sequential test used for shape characterization. Finally, it is worth noting that the use of HBV estimation was found to give more reliable results than the FFT based FastScan. Fully understanding the reasons for this improvement is still an open point.

Figure 20 right presents an estimation of the test shape on the FEM using the minimum dynamic residual expansion method [27, 36]. This inverse problem resolution provides richer insights on the test results using a shape known at all FEM DOF. Here, FEM display uses plane cuts, to give a better visualization of relative motion of internal parts (such as the relative displacements of the pins). With too few accelerometers, model correction is fairly limited for the frequency of interest, so that the estimation hugely relies on the model. With vibrometer measurements, spatial information is notably richer and can be exploited for design orientation [37].

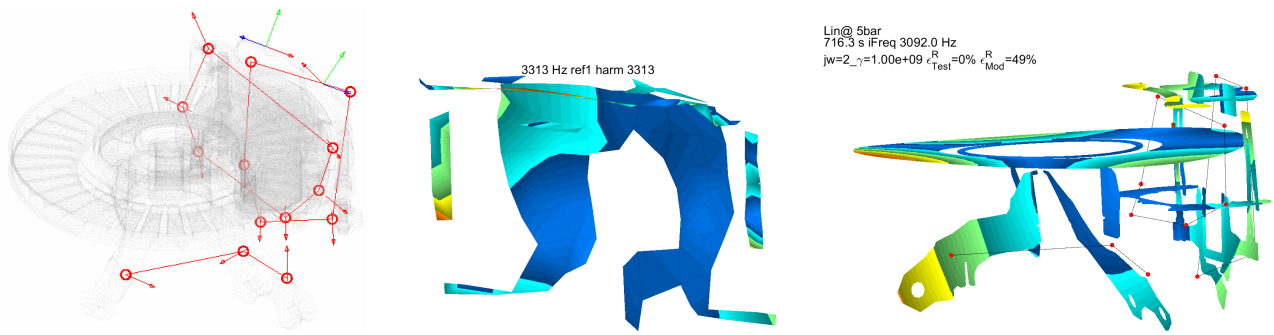

Fig. 20: Left: accelerometer positions on the FEM mesh. Center: sample 3D-SLDV measured shape. Right: expanded test result.

4 Conclusion

Estimation of a HBV signal model provides a methodology to separate slowly varying squeal limit cycle characteristics from remaining broadband noise. The concept is consistent with the expected physical behavior at multiple sensors and was found to be more appropriate than FFT based alternatives. Vibration features (instant frequency and complex shapes) can thus be sampled at a lower frequency (here still a rich 1 kHz is kept) and using lower number of digits, as one does neither expect nor seek high relative precision. This leads to data volume reduction by close to two orders of magnitude.

The methodology is sufficiently robust to be used on full industrial squeal characterization test matrices combining constant torque stops, constant deceleration stops, constant velocity with variable pressure tests, ... The resulting data was used to propose classification strategies with a novel level of detail. In particular, measuring shape continuously enables the clustering of occurrences, not only by frequency and acoustic amplitude, but also by shape.

The definition of a decay ratio leads to the proposition of *transient root locus* analysis. This motivates *continuous parametric tests* giving a characterization of the edges of the instability areas where squeal is intermittent. For the retained case, these transients are very correlated with wheel position, which affects the contact pressure fields as indicated by the bracket/disc distance and torque measurements. The importance of disk micro-geometry has been documented in other studies and the results shown here indicate that relative displacement measurements may be a relevant characterization strategy.

In classical control theory, root locus corresponds to the study of the evolution of poles with changing control gains. Here, the terminology root locus was retained to insist on the fact that the evolution of limit cycle characteristics is coherent with a distributed contact stiffness change (which plays the role of a gain). Simulation results on functional [33] and reduced FEM models could be analyzed using the same HBV estimation procedure than test. This enables consistency analyzes and novel model validation procedures. The associated results will be documented in future publications.

Effects of irregularities viewed as torque impacts, and laser vibrometer dropouts are two sources of measured signal that cannot be represented by the HBV, but their impulsive nature is sufficiently different from the nearly-periodic limit cycle response that one can expect signal estimation techniques to be able to provide an improved estimate. Kalman filter based techniques [24] could probably be used in conjunction with the methodology proposed here to improve initial results in specific configurations, while retaining the advantage of always producing a result.

Outside the experimental characterization of squeal limit cycle, the HBV signal model has many other uses. For non-linear transient computations, it was successfully used to obtain evolution of pad pressure distributions with limit cycle amplitude. For noisy tests with sweep shaker excitation, engine run-up, variable speed imbalance cases, clean estimates of HBV signals could be obtained with a single pass when FFT based methodologies required averaging. Finally, combination of multiple harmonics were used to analyze modulations within the period [38].

Authors' Contributions

Etienne Balmes supervised and contributed to the research and code development; analyzed test results; wrote the paper. Guillaume Martin supervised tests, contributed to code and validation. Guilherme Malacrida performed the tests and analyzed an earlier compaign on the same brake. Guillaume Vermot des Roches was involved in discussions about the relation with FEM simulation strategies where parametric transient studies are analyzed using HBV.

All authors were involved in testing HBV usage on real cases and revision of the manuscript.

Acknowledgements

The SDTools developments linked to squeal testing and simulation included the thesis of G. Malacrida Alves [39] partially funded by ANRT and Hitachi Astemo. The configuration tested corresponds to a pad design chosen to have notably higher squeal occurrences than production brakes.

References

[1] F. Moirot. *Etude de La Stabilité d'un Équilibre En Présence de Frottement de Coulomb*. PhD thesis, Ecole Polytechnique, 1998.

[2] F. Massi, O. Giannini, and L. Baillet. Brake squeal as dynamic instability: An experimental investigation. *The Journal of the Acoustical Society of America*, 120(3):1388–1398, September 2006. ISSN 0001-4966. doi:10.1121/1.2228745.

[3] M. Stender, M. Tiedemann, L. Hoffmann, and N. Hoffmann. Determining growth rates of instabilities from time-series vibration data: Methods and applications for brake squeal. *Mechanical Systems and Signal Processing*, 129, April 2019. doi:10.1016/j.ymssp.2019.04.009.

[4] N. Hoffmann, M. Fischer, R. Allgaier, and L. Gaul. A minimal model for studying properties of the mode-coupling type instability in friction induced oscillations. *Mechanics Research Communications*, 29(4):197–205, July 2002. ISSN 0093-6413. doi:10.1016/S0093-6413(02)00254-9.

[5] G. Vermot des Roches, E. Balmes, R. Lemaire, and T. Pasquet. Design oriented Time/frequency analysis of contact-friction instabilities in application to automotive brake squeal. In *ISMA*, pages 4383–4398, 2010.

[6] M. Stender, S. Oberst, M. Tiedemann, and N. Hoffmann. Complex machine dynamics: Systematic recurrence quantification analysis of disk brake vibration data. *Nonlinear Dynamics*, 97(4):2483–2497, September 2019. ISSN 0924-090X, 1573-269X. doi:10.1007/s11071-019-05143-x.

[7] J. Prezelj, J. Murovec, S. Huemer-Kals, K. Häsler, and P. Fischer. Identification of different manifestations of nonlinear stick–slip phenomena during creep groan braking noise by using the unsupervised learning algorithms k-means and self-organizing map. *Mechanical Systems and Signal Processing*, 166:108349, March 2022. ISSN 0888-3270. doi:10.1016/j.ymssp.2021.108349.

[8] S. Besset, D. Lenoir, and J.-J. Sinou. Brake Squeal Investigations Based on Acoustic Measurements Performed on the FIVE@ECL Experimental Test Bench. *Applied Sciences*, 13(22):12246, January 2023. ISSN 2076-3417. doi:10.3390/app132212246.

[9] F. Massa. *Contributions à l'intégration Des Variabilités En Dynamique Des Structures*. HDR, UVHC, 2022.

[10] A. Lazzari, D. Tonazzi, G. Conidi, C. Malmassari, A. Cerutti, et al. Experimental Evaluation of Brake Pad Material Propensity to Stick-Slip and Groan Noise Emission. *Lubricants*, 6(4):107, December 2018. ISSN 2075-4442. doi:10.3390/lubricants6040107.

[11] M. Krack, L. Panning-von Scheidt, and J. Wallaschek. On the computation of the slow dynamics of nonlinear modes of mechanical systems. *Mechanical Systems and Signal Processing*, 42(1):71–87, January 2014. ISSN 0888-3270. doi:10.1016/j.ymssp.2013.08.031.

[12] G. Kerschen, M. Peeters, J. C. Golinval, and A. F. Vakakis. Nonlinear normal modes, Part I: A useful framework for the structural dynamicist. *Mechanical Systems and Signal Processing*, 23(1):170–194, January 2009. ISSN 0888-3270. doi:10.1016/j.ymssp.2008.04.002.

[13] N. Coudeyras, J. J. Sinou, and S. Nacivet. A new treatment for predicting the self-excited vibrations of nonlinear systems with frictional interfaces: The Constrained Harmonic Balance Method, with application to disc brake squeal. *Journal of Sound and Vibration*, 319(3-5):1175–1199, January 2009. ISSN 0022-460X. doi:10.1016/j.jsv.2008.06.050.

[14] L. Guillot, A. Lazarus, O. Thomas, C. Vergez, and B. Cochelin. A purely frequency based Floquet-Hill formulation for the efficient stability computation of periodic solutions of ordinary differential systems. *Journal of Computational Physics*, 416: 109477, September 2020. ISSN 0021-9991. doi:10.1016/j.jcp.2020.109477.

[15] J. Taghipour, H. Haddad Khodaparast, M. I. Friswell, A. D. Shaw, H. Jalali, et al. Harmonic-Balance-Based parameter estimation of nonlinear structures in the presence of Multi-Harmonic response and force. *Mechanical Systems and Signal Processing*, 162:108057, January 2022. ISSN 0888-3270. doi:10.1016/j.ymssp.2021.108057.

[16] M. Feldman. Hilbert transform in vibration analysis. *Mechanical Systems and Signal Processing*, 25(3):735–802, April 2011. ISSN 08883270. doi:10.1016/j.ymssp.2010.07.018.

[17] S. Mojrzisch, J. Wallaschek, and J. Bremer. An Experimental Method for the Phase Controlled Frequency Response Measurement of Nonlinear Vibration Systems. *PAMM*, 12(1):253–254, December 2012. ISSN 16177061. doi:10.1002/pamm.201210117.

[18] S. Davis and I. Bucher. Automatic vibration mode selection and excitation; combining modal filtering with autoresonance. *Mechanical Systems and Signal Processing*, 101:140–155, February 2018. ISSN 08883270. doi:10.1016/j.ymssp.2017.08.009.

[19] V. Denis, M. Jossic, C. Giraud-Audine, B. Chomette, A. Renault, et al. Identification of nonlinear modes using phase-locked-loop experimental continuation and normal form. *Mechanical Systems and Signal Processing*, 106:430–452, June 2018. ISSN 08883270. doi:10.1016/j.ymssp.2018.01.014.

[20] M. Scheel. Nonlinear modal testing of damped structures: Velocity feedback vs. phase resonance. *Mechanical Systems and Signal Processing*, 165:108305, February 2022. ISSN 0888-3270. doi:10.1016/j.ymssp.2021.108305.

[21] C. Peeters, J. Antoni, Q. Leclère, T. Verstraeten, and J. Helsen. Multi-harmonic phase demodulation method for instantaneous angular speed estimation using harmonic weighting. *Mechanical Systems and Signal Processing*, 167:108533, March 2022. ISSN 08883270. doi:10.1016/j.ymssp.2021.108533.

[22] T. J. Gardner and M. O. Magnasco. Sparse time-frequency representations. *Proceedings of the National Academy of Sciences*, 103(16):6094–6099, April 2006. ISSN 0027-8424, 1091-6490. doi:10.1073/pnas.0601707103.

[23] P. Flandrin, F. Auger, and E. Chassande-Mottin. Time-Frequency Reassignment: From Principles to Algorithms. In A. Papandreou-Suppappola, editor, *Applications in Time-Frequency Signal Processing*, pages 179–204. CRC Press, 1 edition, October 2018. ISBN 978-1-315-22001-7. doi:10.1201/9781315220017-5.

[24] N. Peyret, J.-L. Dion, and G. Chevallier. A framework for backbone experimental tracking : Piezoelectric actuators, stop-sine signal and Kalman filtering. *Mechanical Systems and Signal Processing*, 78:28–42, October 2016. ISSN 0888-3270. doi:10.1016/j.ymssp.2015.09.020.

[25] C. Hubert, Y. E. Attaoui, N. Leconte, and F. Massa. A coupled finite element-discrete element method for the modelling of brake squeal instabilities. *European Journal of Mechanics - A/Solids*, 108:105427, November 2024. ISSN 0997-7538. doi:10.1016/j.euromechsol.2024.105427.

[26] G. Raze, G. Abeloos, and G. Kerschen. Experimental continuation in nonlinear dynamics: Recent advances and future challenges, July 2024.

[27] G. Martin. *Méthodes de Corrélation Calcul/Essai Pour l'analyse Du Crissement*. Ph.D. thesis, CIFRE SDTools, Arts et Metiers ParisTech, Paris, March 2017.

[28] A. Saxena, M. Prasad, A. Gupta, N. Bharill, O. P. Patel, et al. A review of clustering techniques and developments. *Neurocomputing*, 267:664–681, December 2017. ISSN 09252312. doi:10.1016/j.neucom.2017.06.053.

[29] P. Å. Wedin. On angles between subspaces of a finite dimensional inner product space. In B. Kågström and A. Ruhe, editors, *Matrix Pencils*, volume 973, pages 263–285. Springer Berlin Heidelberg, Berlin, Heidelberg, 1983. ISBN 978-3-540-11983-8 978-3-540-39447-1.

[30] A. K. Jain. Data clustering: 50 years beyond K-means. *Pattern Recognition Letters*, 31(8):651–666, June 2010. ISSN 01678655. doi:10.1016/j.patrec.2009.09.011.

[31] M. Volvert and G. Kerschen. Phase resonance nonlinear modes of mechanical systems. *arXiv:2010.14892 [math]*, October 2020.

[32] N. Hoffmann and L. Gaul. Effects of damping on mode-coupling instability in friction induced oscillations. *ZAMM*, 83(8): 524–534, August 2003. ISSN 00442267, 15214001. doi:10.1002/zamm.200310022.

[33] G. M. Alves, E. Balmes, and G. Martin. Analysis of a brake squeal functional model using a linear parameter varying perspective. In *INTER-NOISE and NOISE-CON Congress and Conference Proceedings*, volume 270, pages 473–484, 2024.

[34] G. Martin, E. Balmes, G. Vermot Des Roches, and T. Chancelier. Squeal measurement with 3D Scanning Laser Doppler Vibrometer: Handling of the time varying system behavior and analysis improvement using FEM expansion. In *ISMA*. KUL, September 2018.

[35] B. Witt, D. Rohe, and T. Schoenherr. Full-Field Strain Shape Estimation from 3D SLDV. In C. Niezrecki, J. Baqersad, and D. Di Maio, editors, *Rotating Machinery, Optical Methods & Scanning LDV Methods, Volume 6*, pages 31–45. Springer International Publishing, Cham, 2019. ISBN 978-3-030-12934-7 978-3-030-12935-4. doi:10.1007/978-3-030-12935-4-4.

[36] P. Ladeveze, G. Puel, A. Deraemaeker, and T. Romeuf. Validation of structural dynamics models containing uncertainties. *Computer methods in applied mechanics and engineering*, 195(4):373–393, 2006.

[37] G. Martin, E. Balmes, T. Chancelier, S. Thouviot, and R. Lemaire. A Structural Dynamics Modification Strategy based on Expanded Squeal Operational Deflection Shapes. In *EuroBrake 2022 - Technical Content*. FISITA, May 2022. ISBN 978-1-916025-95-0. doi:10.46720/EB2022-TSD-009.

[38] G. Malacrida Alves and E. Balmes. A time varying system perspective on rubber mount tests. In *ISMA*, Leuven, Belgium, 2022. KUL.

[39] G. Malacrida Alves. *Experimental Modal Analysis of Time Varying Non-Linear Systems. Application to Brake Squeal.* Ph.D. thesis, CIFRE SDTools, Arts et Metiers ParisTech, Paris, To be defended Jan 2025.